Response to Referees and Comments

Iodine oxide in the global marine boundary layer

C. Prados-Roman, C. A. Cuevas, T. Hay, R. P. Fernandez, A. S. Mahajan, S-J. Royer, M. Galí, R. Simó, J. Dachs, K. Großmann, D. E. Kinnison, J-F. Lamarque and A. Saiz-Lopez

We would like to thank both anonymous referees as well as Dr. Guzman for their constructive comments and also for their appreciation of our work. In the following we present our point-by-point answer (Authors Comment- AC) to each of their remarks on our manuscript (Referee Comment- RC, or Short Comment- SC). Attached to this document we also include the new versions of the manuscript and of the supplementary information indicating the changes in red.

****

Anonymous Referee #1

****

RC:

This is a very good paper which is suitable for publication in ACP, essentially as is. I did not find any substantive points to raise, but the authors may wish to consider one or two points made below.

The paper provides a very good synthesis of field data of IO measured by the MAXDOAS method during several marine cruises, spanning a good range of geographical locations worldwide. The observed levels are consistent with the source term for iodine being predominantly from the reaction of ozone with iodide in sea-water and subsequent chemical conversions and release of photolabile I, mainly in the form of HOI. Organic I (from measurements of RI species where available, otherwise estimated from global models) are a minor source of I – at least outside of the polar regions, and this study shows that the % contribution towards I production between inorganic and organic source gases varies from location to location. All the measurements are made using the MAX-DOAS method, which has a complex retrieval algorithm to generate slant column densities, and assumptions are then made regarding the sampling depth to convert to mixing ratios. In that regard including measurements using other methods based on fundamentally different principles of operation would be desirable in the future.

Perhaps the most important conclusion from this paper is that although the amounts of IO vary a little (0.4-1 ppt during the Malaspina cruise and other values close to this from other cruises), IO is present everywhere (polar regions not included in this analysis), demonstrating that iodine production from the oceans is a truly global phenomenon, and needs to be taken into account in Earth System Models, to properly calculate O3, HOx and other important intermediates which control, for example, the lifetimes and abundances of some non-CO2 greenhouse gases (CH4). The levels also show that the recently developed parameterisation for the release of inorganic I from the ocean is able to account for the typical levels observed (with the source rate varying owing to variations in O3, SST, wind speed and sea-water I-). Direct measurements of HOI mixing ratios in the future though above the oceans would be highly desirable top confirm this.

AC:
We are grateful to Referee #1 for his/her comments and suggestions. We agree on his/her recommendations regarding objectives for future studies. We also consider that new measurements as well as a diversity of the employed measurement techniques would serve the purpose of a better understanding of the background chemistry despite the intrinsic uncertainties linked to each technique. We hope the scientific community will be encouraged by her/his suggestions. In the following we proceed to answer each of his/her comments referred to our manuscript.

Uncertainties are discussed in the supplementary material, and briefly in the main paper, but some mention of the uncertainty of the measurements should be given in the abstract following the range of values that are given. This will allow the reader to gauge how significant the observed levels of IO are compared with the instrumental uncertainties or detection limits (which will include the uncertainty in the mixing depths assumed to convert slant columns into mixing ratios, this depth varying from study to study).

AC:
As suggested, the measurement's uncertainty is now added also in the abstract ("30% uncertainty"). As the referee mentions, further details regarding uncertainties are already provided in the Supplementary Information (Sect. 1.1.2).

Page 22222, line 19, can the elevation angles also include the range of altitudes this corresponds to.

AC:
In general, the altitude sensed by a given MAX-DOAS elevation angle depends on diverse parameters like the physicochemical properties of the atmosphere, the ground albedo, the targeted wavelength and the particularities of the aimed trace gas itself. Since the MAX-DOAS technique has been widely used for years and there is a vast bibliography providing these sorts of details (e.g., Platt and Stutz, 2008 and references therein), we consider that including additional information regarding the technique itself could confuse the reader since in fact no vertical profile is intended in our work. If further information on the technique is needed, as suggested on our manuscript (Page 22222, lines 11-14) we recommend to refer to former works where detailed sensitivity studies were investigated for particularities such as the last scattering altitude for a given aerosol load and elevation angle (e.g., Hönninger et al., 2004). In the case of Malaspina and as stated in the manuscript (Page 8, line 5), photons gathered at an elevation angle of 2º referred to a mean last scattering altitude of 600 m.

****

Anonymous Referee #2

****

RC:
The manuscript by Prados-Roman et al. combines field observations of iodine monoxide with a 3D global model analysis of the most likely sources of reactive iodine in the marine boundary layer. The data originates from multi-axis DOAS measurements acquired during the Malaspina global circumnavigation in 2010. IO mixing ratios averaged in the lowest ~600m of the atmosphere are reported. In addition, IO data from earlier field experiments are included in the study. The global 3D atmospheric chemistry model CAM-Chem with various oceanic iodine source parameterizations was used to compare to the data. The

parameterization including organic iodine precursors and an inorganic ocean surface source of I2 and HOI, according to the parameterization of MacDonald et al., appears to match the data best. The authors thus conclude that an abiotic marine surface source, which accounts for 75% of the emitted iodine, is globally active.
This is a well written that presents interesting data and model results and carefully argues for the presence of an abiotic iodine source at the ocean surface. However, there are a number of issues that require more detailed explanations before the manuscript can be published in ACP:

AC: We kindly thank Referee #2 for his/her review which will help to improve our manuscript. We now proceed to answer her/his comments point-by-point.

1) A number of filtering procedures were applied to the data. It appears that after the filters have been applied, no IO DSCD observations below ~1×10^{13} molec. cm^{-2} remain (Figure 3b). The insert in Figure 3b seems to indicate that all data with a 10° were excluded, even in scans where lower viewing elevation angles passed the filters. The exclusion of the larger viewing elevation angle data is rather counter-intuitive as MAXDOAS retrievals often lead to smaller, or at least similar, residual RMS for larger elevation viewing angles and no other filter should remove these data points if the smaller elevation angles passed the filters. This must be explained in more detail. While the reported IO mixing ratios were only derived from the 2° observations, the results in Figure 3b open the question on how appropriate the filtering procedures were. The fact that only 2° elevation angle data was used to derive the mixing ratios should be mentioned in the main text and not just in the supplement.

AC: We particularly thank this comment since, after having a closer look to the inset in Figure 3b addressed by the referee, we've realized there is an error in the colour of the empty squares (i.e., data below quality filters). By mistake the empty squares shown in the inset for the elevation angle of 10º presents the same colour code as for higher angles. This will be corrected in the new version of the manuscript. We do apologize for the mistake. Please bear in mind that the colour code for the main plot as well as for filled circles of the inset is correct. Indeed, as correctly stated by the referee and as shown in Fig. 3b by the filled circles (i.e., data above quality filters) not only in the main plot but also in the inset, there were times when measurements at high elevation angles were in fact statistically relevant.
Please note that, similarly to former studies (e.g., Mahajan et al., 2012), the quality filter applied to our measurements includes a diverse set of filters detailed in the SI such as the SZA, RMS, clouds, wind direction, etc., rendering this quality filter as a rather strict filter (necessary on the other hand given the size of Malaspina's dataset).
As suggested by the referee, besides the information that is already included in the SI, in the new manuscript the sentence (last paragraph of Sect. 3.1) "Therefore the values reported in Fig. 4 should be considered as the mean IO vmr in each of the aforementioned altitude ranges" will be completed with "linked to a given elevation angle (e.g., 2º in the case of Malaspina 2010)."

2) One of the main factors in converting MAX-DOAS column densities into mixing ratios is the assumption of the boundary layer height. The accuracy of the assumption of a 600m high boundary layer and the height of the boundary layer in the model merit a more detailed discussion. Ideally, the comparison between the observations and the model should be made using a vertical column density, perhaps in the lowest 1000m of the atmosphere, as this quantity would eliminate the boundary layer height uncertainty and thus be more closely related to the emissions.

AC: During Malaspina 2010 the upper layer of the sensed "column" with the MAX-DOAS instrument (referred to as MBL in the manuscript) was defined by the mean last scattering altitude (LSA) of the photon reaching the detector when the MAX-DOAS was measuring at an elevation angle of 2º. This LSA was calculated by means of sensitivity studies performed with the radiative transfer model NIMO (Hay et al., 2012). Thus, there was no need of estimating the height of the MBL per se. Instead, the LSA for the given elevation angle was modelled considering the measurements of O_4 at same elevation angle (note that the vertical distribution of O_4 in the atmosphere is a known parameter). This is now made clearer in the Supplementary Information (Sect. 1.1.2) by completing the sentence (line 26) "with 600 m as the mean last scattering altitude (LSA)" with "of the photon reaching the detector at that elevation angle defining the upper layer of the sensed "column" (i.e., MBL)". As stated in the manuscript (Page 8, line 5), based on this mean LSA modelled during the campaign, the Malaspina's IO mixing ratios presented were therefore regarded as representative of the first 600 m of the atmosphere (see also Fig. 1 below).

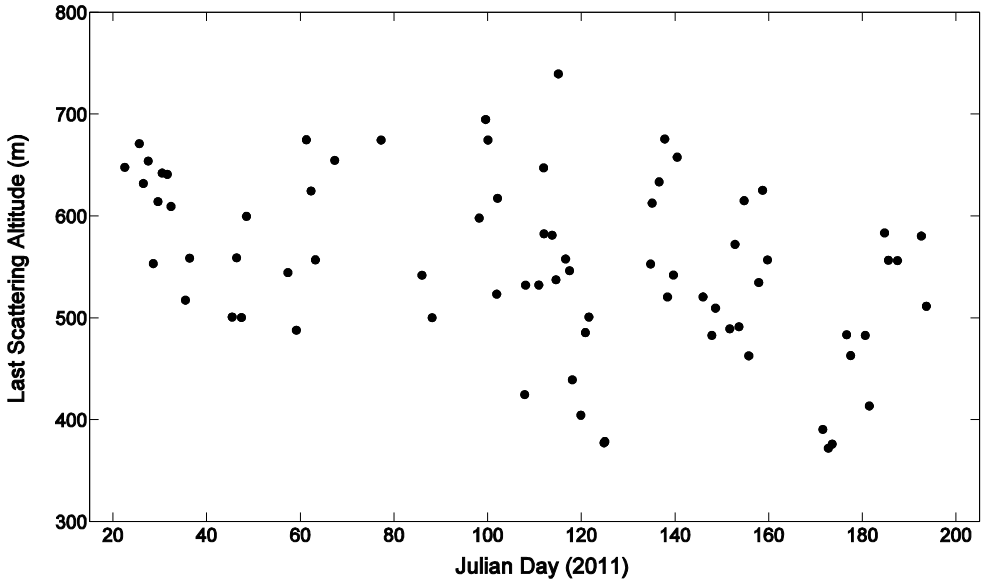

Fig. 1: Modelled mean last scattering altitude (2º elevation angle) during Malaspina's expedition.

Note that this same altitude range was considered for the CAM-Chem output when comparing measured and modelled IO mixing ratios in the manuscript (i.e., 0-600 m). The same applies for the other campaigns bearing in mind that each campaign employed a different elevation angle for the retrieval of mixing ratios, yielding therefore a different intrinsic definition of the "column" sensed (MBL) for each campaign. This is now made clearer in the manuscript by completing the sentence (first paragraph of Sect. 3.2) "The performance of the model was evaluated by comparing modelled and observed IO mixing ratios in the MBL" with "for the aforementioned particular altitude range sensed during each campaign".

3) Does the 3D model include clouds? If so, was model data filtered in the same way as observations? If not, could there be a bias in the model as cloudy days were excluded from the data? This needs a more detailed explanation.

AC: Generally speaking, the cloud formation, microphysics and precipitation schemes are indeed parameterised in CAM-Chem. The current version of the model includes improvements on the

representation of deep convection, plume dilution and cloud fraction distributions by means of introducing a Convective Momentum Transport scheme. As mentioned in the manuscript (Sect. 2.2), we recommend the reader to refer to the study of Lamarque et al., (2012) for further details on the model.

In our work, as stated in the manuscript (last paragraph of Sect. 2.2.1) and similarly to the study of Saiz-Lopez et al. (2014), we considered a specified dynamic mode based on the meteorological fields from a previous climatological simulation representative of the 2000-2010 decade. Therefore the geographical and temporal evolution of the cloud fields and precipitation rates used were climatological (i.e., not representative of the particular meteorology of any specific year). Thus, the model cloudiness cannot be compared directly to the specific conditions of the Malaspina 2010 cruise. Instead, based on that climatology (i.e., the most probable situation from a statistical point of view), we applied a temporal mask when computing the monthly model averages to consider only day-time mixing ratios at any given latitude and longitude in the same way as for the experimental data. It is worth mentioning that, within all the unknowns and uncertainties related to the implementation of the iodine chemistry into a 3D global model, the presence of clouds are only a minor component and, in any case, their stronger impacts are associated to the washout efficiency by in-cloud and below cloud scavenging of inorganic iodine species (Lamarque et al., 2012; Saiz-Lopez et al., 2014). Note that our work shows that, independently of the absolute levels that could be affected by unaccounted clouds in the model, both modelled and measured mixing ratios are compatible and indicate the ubiquitous presence of IO in the MBL.

In summary, this manuscript is well suited for publication in ACP. I recommend publication after the issues described above have been addressed.

AC: We appreciate Referee#2's recognition. We consider with this answer we have covered all the issues addressed by the referee.

****

Dr. Guzman

****

SC:

The manuscript "Iodine oxide in the global marine boundary layer" by Prados-Roman et al. presents multi-axis DOAS measurements of IO radical mixing ratios (< 1 pptv, altitude ≤ 600 m) performed over the marine boundary layer (MBL). A combined analysis with other field data suggests that iodine driven chemistry is of global importance over the oceans. A 3D CAM-Chem model discerning the contribution of organic and inorganic emissions (specifically hypoiodous acid and molecular iodine), and their associated geographical dependence, estimates that 75% of the total iodine oxide budget if of abiotic origin in the global MBL. This manuscript is an important contribution to understand the oxidizing capacity of the atmosphere and presents new data to support an abiotic mechanism is operative over open ocean waters. However, it would be important to consider in this manuscript a recent laboratory study by Pillar et al. (Environ. Sci. Technol., 2013, 47, 10971−10979, http://dx.doi.org/10.1021/es401700h) that indicates how sea spray aerosol production and in-situ oxidation produces hypoiodous acid and molecular iodine. Guzman et al. (J. Phys. Chem. A, 2012, 116, 5428–5435, http://dx.doi.org/10.1021/jp3011316) studied the

enrichment of halides during aerosolization of seawater mimic samples providing new insights about how concentration effects could be included in a model. More importantly, it would be interesting to discuss in the final version of the manuscript to be published in ACP how reactions at the air−water interface of sea spray, followed by transfer of reactive products to the gas-phase (Environ. Sci. Technol., 2013, 47, 10971−10979, http://dx.doi.org/10.1021/es401700h) contributes to the model presented. In addition, it would be important to connect the manuscript with Pillar et al. previously proposal indicating that 1) the actual source of reactive iodine species will vary geographically., 2) the production of sea spray will be sensitive to local conditions, particularly surface winds, 3) the production of iodine will depend on factors such as temperature, humidity, and the concentration of halogen species, and 4) 3D models should be chosen over 1D models to approach this problem.

AC: We thank Dr. Guzman for his appreciation of our work and comments. Note that the references Dr. Guzman addresses relate to the heterogeneous chemistry behind marine aerosol. Our work focuses on the measured ubiquity of IO in the MBL and on modeling the oceanic inorganic vs. organic contribution to the emitted iodine. Although the model used in our work included recycling of HOI, $IONO_2$ and INO_2 in aerosols (see also Saiz-Lopez et al., 2014), getting into the particularities of the different pathways such as the mechanism proposed in the study of Pillar et al. (2013) is actually out of the scope of our current study. Nevertheless, in agreement with Dr. Guzman, we also consider the interactions of halides and sea spray a very interesting topic worth looking at in future works where both measurements and model studies could be combined.

Iodine oxide in the global marine boundary layer

C. Prados-Roman[1], C. A. Cuevas[1], T. Hay[1], R. P. Fernandez[1,*], A. S. Mahajan[1,], S-J. Royer[2], M. Galí[2,†], R. Simó[2], J. Dachs[3], K. Großmann[4], D. E. Kinnison[5], J-F. Lamarque[5] and A. Saiz-Lopez[1]**

[1]{Atmospheric Chemistry and Climate Group, Institute of Physical Chemistry Rocasolano (CSIC), Madrid, Spain}.

[2]{Institute of Marine Sciences, (CSIC), Barcelona, Spain}.

[3]{Institute of Environmental Assessment and Water Research (CSIC), Barcelona, Spain}.

[4]{Institute of Environmental Physics, University of Heidelberg, Germany}.

[5]{Atmospheric Division, NCAR, Boulder, CO, USA}.

[*]{now at: National Scientific and Technical Research Council (CONICET), UTN-FR Mendoza/ICB-UNCuyo, Mendoza, Argentina}.

[**]{now at: Indian Institute of Tropical Meteorology, Pune, India}.

[†]{now at: Takuvik (UL/CNRS), Quebec, Canada}.

Correspondence to: a.saiz@csic.es.

Abstract

Emitted mainly by the oceans, iodine is a halogen compound important for atmospheric chemistry due to its high ozone depletion potential and effect on the oxidizing capacity of the atmosphere. Here we present a comprehensive dataset of iodine oxide (IO) measurements in the open marine boundary layer (MBL) made during the Malaspina 2010 circumnavigation. Results show IO mixing ratios ranging from 0.4 to 1 pmol mol^{-1} (30% uncertainty) and, complemented with additional field campaigns, this dataset confirms through observations the ubiquitous presence of reactive iodine chemistry in the global marine environment. We use a global model with organic (CH_3I, CH_2ICl, CH_2I_2 and CH_2IBr) and inorganic (HOI and I_2)

iodine ocean emissions to investigate the contribution of the different iodine source gases to the budget of IO in the global MBL. In agreement with previous estimates, our results indicate that, globally averaged, the abiotic precursors contribute about 75% to the iodine oxide budget. However, this work reveals a strong geographical pattern in the contribution of organic vs. inorganic precursors to reactive iodine in the global MBL.

1 Introduction

The atmospheric relevance of reactive halogens became clear decades ago when their potential to catalytically destroy ozone (O_3) was first recognised in the polar stratosphere (Molina and Rowland, 1974) and later on in the troposphere (e.g. Barrie et al., 1988). Halogens are also known to affect the NO_x (NO, NO_2) and HO_x (HO, HO_2) partitioning and the lifetime of organic compounds, to alter the sulphur and mercury cycles and, in the case of iodine oxides, to form ultra-fine particles in coastal areas (Saiz-Lopez and von Glasow, 2012 and references therein).

Since the first study to deal with the tropospheric relevance of inorganic iodine (Chameides and Davis, 1980), major efforts have been made to detect reactive iodine species in their main source region: the oceans (Saiz-Lopez et al., 2012 and references therein). Several field campaigns in scattered marine environments have aimed at detecting iodine oxide - beacon for the presence of active iodine chemistry- and determining the nature and strength of organic and inorganic source gases of iodine (referenced hereafter as OSG, ISG, respectively). Air-sea fluxes of iodocarbons (CH_3I, CH_2I_2, CH_2ICl and CH_2IBr, C_2H_5I, 1-C_3H_7I, 2-C_2H_7I) have been reported (Carpenter et al., 2012), but in general observations were insufficient to explain measured IO concentrations in the MBL, implying the existence of an abiotic ocean source of iodine (Mahajan et al., 2010; Jones et al., 2010; Mahajan et al., 2012; Gómez Martín et al., 2013a; Großmann et al., 2013; Lawler et al., 2014). In several one-dimensional model studies simulated emissions of molecular iodine (I_2) were used to fit IO observations (e.g. Mahajan et al., 2010; Großmann et al., 2013), however the recent work of Lawler et al. (2014) with the first observation of I_2 in the remote MBL, confirmed that the emission of I_2 is still insufficient to explain the observed levels of IO. Recently, the study of Carpenter et al. (2013) has experimentally confirmed that not only I_2 is emitted naturally from the oceans but also, and mainly, hypoiodous acid (HOI). In that study and in the subsequent work of MacDonald et al. (2014), the authors have confirmed through laboratory work that the oceanic emission of

ISG (HOI and I_2) follows the deposition of tropospheric O_3 to the oceans and its reaction with aqueous iodide (I_{aq}^-, Garland et al., 1980), and they proposed a parameterisation for ocean ISG emissions dependent on O_3, wind speed (ws) and sea surface temperature (SST).

In this work, we present a comprehensive map of IO observations in the global MBL showing the ubiquity of this radical in the marine environment. Moreover, by means of a global model including OSG and ISG oceanic emissions; we investigate the geographical emission patterns of both iodine precursors and their contribution to the IO budget in the marine environment. Section 2 details the measurement campaign of Malaspina 2010 and provides information on the chemical model used throughout this work. Section 3 presents the results of the IO observations and the modelling studies, and Section 4 concludes this work.

2 Measurements and model

In the following we present the setup of the O_3 and IO measurements during the Malaspina 2010 expedition as well as the model schemes used in this study.

2.1 Measurements during the Malaspina 2010 circumnavigation

From December 2010 until July 2011 the Spanish research vessel Hesperides circumnavigated the World´s oceans within the framework of the Malaspina 2010 project. The main objectives of this interdisciplinary campaign were to investigate the biogeochemistry, physical properties and microbiological biodiversity of the oceans; the genetic diversity of the deep-ocean and the exchange of trace gases and pollutants with the atmosphere; and assessing the impact of global change in the ocean. The different legs of the cruise and the docking dates are indicated in Table 1.

A Multi-Axis Differential Optical Absorption Spectroscopy instrument (MAX-DOAS; Platt and Stutz, 2008) and a commercial 2B-205 ozone monitor, along with a GPS, were deployed aboard the vessel in order to investigate the presence of atmospheric trace gases such as IO, O_3, BrO, HCHO and CHOCHO in the MBL. Herein we focus on the observations of IO and O_3 during the campaign.

2.1.1 Surface ozone

The ozone monitor was installed in the ship's bridge with a 5 m long Teflon-lined inlet tube from the upper deck, well forward of the exhaust stacks (~15 m above sea level (m.a.s.l.)). The inlet was placed just above the railing in the air coming from the front of the ship, avoiding sampling air from the ship's boundary layer. Due to GPS communication errors, our data compilation started on 21/02/2011 (2^{nd} leg) and finished on 12/07/2011.

The ozone volume mixing ratios (vmr) observed during Malaspina 2010 are presented in Fig. 1a along with the ancillary measurements of relevance for the present work (i.e., SST and ws; Fig. 1 and Table 2). Simulations of the 5-day backward trajectories of the air masses arriving at the ship's track are provided in Fig. 2, showing the typical non-continental origin of the air masses sensed during the cruise.

2.1.2 Iodine oxide

Aiming at the detection of IO along the Malaspina's track, a MAX-DOAS instrument was installed on the second deck near the rear of the ship (~10 m.a.s.l.). Briefly, these instruments measure the intensity of scattered light in the UV-VIS range entering a scanning telescope at several precise viewing angles and have been widely used for atmospheric composition research (Platt and Stutz, 2008). Thus only a summary of the particular MAX-DOAS instrument mounted on the Hesperides research vessel is given hereafter. For details regarding the MAX-DOAS technique please refer to the work of, e.g., Platt and Stutz (2008) and Hönninger et al. (2004) and for further details of our ship-based MAX-DOAS instrument please see Mahajan et al. (2012).

Briefly, in the case of the Malaspina's MAX-DOAS instrument, the scanning telescope was housed in a weatherproof metal chamber with a flat UV-transmitting acrylic window, with a sunshade to reduce spectral effects on the window. The telescope unit (built by the New Zealander National Institute of Water and Atmospheric Research-NIWA) was mounted on a gimbal table to compensate for the pitch and roll of the ship. The gimbal dampened the effective oscillations in telescope elevation angle to ±1º for most of the cruise and ±2º in rough conditions. In addition, a high accuracy (±0.1º), fast response (0.3 s) inclinometer was used to log the residual oscillations in order to correct the elevation angles. Only true angles within 0.2º of each prescribed elevation angle were used for analysis. The azimuth viewing direction was towards the ship's bow (20º anticlockwise) to minimize exhaust emissions in the

line of sight. The scanning telescope consisted of a rotating diagonal mirror driven by a stepper motor and a 50.8 mm diameter fused silica lens with a focal length of 200 mm, giving a field of view of 0.5º. The light was focused onto a 5 m long 19 optic fibre bundle leading to a Princeton Instruments SP500i spectrometer with a Princeton Instruments Pixis 400B CCD camera. A 600 grooves mm^{-1} grating was used, giving approximately an 80 nm spectral window and a spectral resolution of 0.5 nm FWHM. Spectra were recorded for a short exposure time of 1 s at each discrete elevation angle (2, 4, 6, 8, 10, 15, 30 and 90º) in order to minimize potential deviations in angle due to the ship's movement. The scan sequence was repeated every 2 min and after every 10 cycles the grating was shifted between the two wavelength regions, centred on 358 nm (UV spectral range) and 440 nm (VIS spectral range). Results presented in this work correspond to the VIS channel, where IO could be measured (see Sect. 3.1).

2.2 Modelling the oceanic emissions of reactive iodine precursors

We implemented the experimentally derived ocean fluxes of ISG (Carpenter et al., 2013; MacDonald et al., 2014) into the global chemistry-climate model CAM-Chem (Community Atmospheric Model with Chemistry, version 4.0; Lamarque et al., 2012), which already included a validated OSG emissions inventory and a state-of-the-art halogen chemistry scheme (Ordónez et al., 2012). The on-line ISG flux formulation, based on the studies of Carpenter et al. (2013) and MacDonald et al. (2014), was performed considering the instantaneous modelled levels of surface O_3, SST and ws in each of the model grid-boxes over the oceans (i.e., imposing an ocean mask). In the following we summarise the model schemes used in this work. Further details on the particular implementation of the ISG parameterisation into the CAM-Chem model are given in Prados-Roman et al. (2014), whereas the general model setup is described in the study of Lamarque et al. (2012).

2.2.1 Model schemes

Throughout this work, two different pairs of simulations were performed in order to evaluate the model, to identify the contribution of OSG/ISG fluxes and to estimate the iodine burden of the MBL. A brief description of the simulations used in this study is given below.

(1) *Base-Organic runs.* In the *Base run*, simulations were performed considering the oceanic emission of organic and inorganic iodine precursors. Based on previous publications, the OSG inventory of very-short lived iodocarbons (OSG= CH_3I,

CH_2I_2, CH_2IBr and CH_2ICl) was considered (Ordónez et al., 2012), while the ISG computation of HOI and I_2 was used as described in the study of Prados-Roman et al., 2014. In order to distinguish the contribution of the inorganic and the organic iodine source gases to the IO budget in the MBL, the *Organic* scheme included only the abovementioned OSG (by forcing the inorganic emissions to be null). Hence, the contribution of ISG to the IO budget in the MBL (i.e., IO_{ISG}) was defined as the difference between the IO vmr obtained in the MBL after the *Base run* ($IO=IO_{ISG+OSG}$), and the IO vmr obtained after the *Organic run* (i.e., IO_{OSG}). That is IO_{ISG}= (IO) - (IO_{OSG}); and the relative contribution of ISG to IO was defined as (IO_{ISG})/(IO) in percentage. Similarly, the contribution of each individual iodocarbon to the budget of IO was investigated.

(2) *NoPhot-Phot runs.* It is known that the self-reaction of IO in pristine conditions yields the formation of higher oxides (I_2O_x, x=2, 3 or 4). However, once formed, the reaction pathways of these compounds are still not well understood. One possibility is their nucleation into ultra-fine particles as observed in coastal areas (Gómez Martín et al., 2013b). Those conditions were however not representative of the Malaspina expedition since most of the marine atmosphere crossed was representative of open ocean environment. A possible pathway for Malaspina's conditions was the photodissociation of those I_2O_x into OIO+I, OIO+IO or OIO+OIO as previously modelled for the Antarctic (Saiz-Lopez et al., 2008) and global marine troposphere (Saiz-Lopez et al., 2014), which would therefore result in additional reactive iodine in the MBL. The so-called *Phot run* included I_2O_x photolysis while the simulation excluding such photolysis was referred to as *NoPhot run*. Note that, unless stated otherwise, in the aforementioned *Base-Organic* schemes the I_2O_x were not allowed to photolyse but, once formed, they were lost by thermal decomposition or to pre-existing aerosols instead.

All simulations were performed with a horizontal grid resolution of 1.9º (latitude) × 2.5º (longitude) and 26 hybrid vertical levels (0-40 km), and considered the SST and sea-ice boundary conditions representative of year 2000 (Rayner et al., 2003). Note that, since the model was not run with specified dynamics, simulations are not representative of the meteorology of any specific year. Thus, unless stated the opposite, the model results presented in this work correspond to 24 h annual averages.

3 Results and discussions

In this section we present the observations of IO in the MBL and compare them to different model runs. Furthermore, we investigate the contribution of the OSG and ISG fluxes to the IO budget in the MBL.

3.1 Observations of IO in the global marine boundary layer

During Malaspina 2010 IO was detected above instrumental detection limit (1.2-3.5x10^{13} molec cm^{-2}) in all marine environments sampled. Figure 3 shows a typical IO spectral fit during that expedition and the IO differential slant column densities (dSCD) measured along the cruise track. Note that diverse filters were used in this dataset for quality assurance (e.g., cloud and wind direction filters). Following previous studies and using only IO dSCD above the quality filters, the IO mixing ratios were inferred by the well-established "O_4 method" (Wagner et al., 2004), after validating results of several days with a radiative transfer model (RTM) (e.g., Mahajan et al., 2012; Gómez Martín et al., 2013a). Particular details on these procedures (IO spectral and vmr retrieval) as well as the quality filters applied are provided in the Supplementary Information (SI).

Overall, during the Malaspina expedition the IO radical was constantly observed in the daytime MBL over three oceans and both hemispheres. The IO vmr integrated in the MBL ranged between 0.4 and 1 pmol mol^{-1} (detection limit of ~0.2 pmol mol^{-1}), with lower values measured over the South Atlantic waters and with the highest levels in the marine region west of Mexico. Figure 4 shows the averaged daytime IO vmr of the Malaspina dataset, along with IO vmr obtained from former field campaigns: Cape Verde (Read et al., 2008; Mahajan et al., 2010), HaloCAST-P (Mahajan et al., 2012), CHARLEX (Gómez Martín et al, 2013a) and TransBrom (Großmann et al., 2013). Note that the IO vmr reported for each of these campaigns are by definition intrinsically linked to the specific viewing geometry of each DOAS instrument (Platt and Stutz, 2008). During the Cape Verde campaign a Long Path-DOAS instrument was used with a fixed light path at 10 m.a.s.l. (Read et al., 2008; Mahajan et al., 2010). In all the other campaigns shown in Fig. 4, MAX-DOAS instruments were employed. Given the different viewing elevation angles and instrumental setup, each of those MAX-DOAS instruments sensed a different part of the MBL (Platt and Stutz, 2008; Hönninger et al., 2004; Wagner et al., 2004). Although sensitivity RTM studies performed during each of those MAX-DOAS campaigns agreed on a decreasing vertical profile of IO in

the MBL, the generally poor information content of the measurements hindered the vertical resolution of the inferred IO vmr vertical profiles and the reported vmr were therefore linked to a given sensed layer; particularly 0-200 m during HaloCAST-P and TransBrom (Mahajan et al., 2012; Großmann et al., 2013), 0-1200 m during CHARLEX (Gómez Martín et al., 2013a) and 0-600 m during Malaspina (this work, SI). Therefore the values reported in Fig. 4 should be considered as the mean IO vmr in each of the aforementioned altitude ranges linked to a given elevation angle (e.g., 2º in the case of Malaspina). Note that, despite these unavoidable retrieval limitations, Fig. 4 proofs the ubiquity of IO in the global MBL and hence the presence of reactive iodine chemistry in all sub-polar marine environments.

3.2 Observations vs. model

Figure 4 shows the most comprehensive map of IO observations in the remote marine environment. We now use these observations together with the CAM-Chem model to evaluate the geographical distribution of IO in the MBL. The performance of the model was evaluated by comparing modelled and observed IO mixing ratios in the MBL for the aforementioned particular altitude range sensed during each campaign. Note that, as mentioned above, a key parameter in the model setup is the flux of ISG, which depends mainly on O_3 and ws (Carpenter et al., 213; MacDonald et al., 2014). Hence, even though Fig. 4 shows IO measurements from 5 different field campaigns, surface O_3, ws and IO were not measured simultaneously during HaloCAST-P and TransBrom campaigns. Thus, only the campaigns of Malaspina, CHARLEX and Cape Verde were chosen for comparison with the model. Figure 5 presents this comparison exercise, where the IO vmr observations in three oceans and both hemispheres are juxtaposed to the model output after the *Organic* scheme and after the *Base* run considering the *NoPhot* and the *Phot* schemes. For this exercise the model was sampled at the same time (month) of the year and geolocation as the measurements (considering the model grid resolution of 1.9º latitude x 2.5º longitude). Note that the low IO vmr resulting after the *Organic* run remains basically unaltered despite the photolysis scheme considered. Thus for simplicity only the *Organic-NoPhot* output (i.e., *Organic* run) is shown in Fig. 5.

Considering the ISG emissions, along with OSG, the model reproduces satisfactorily the IO observations (Fig. 5). Note that, as found in the *Organic* run, the emission of OSG alone explains on average only ~25% of the IO levels observed over the different oceans, percentage that agrees well with previous one-dimensional model studies performed at specific marine environments (Mahajan et al., 2010; Jones et al., 2010; Mahajan et al., 2012;

Gómez Martín et al., 2013a; Großmann et al., 2013; Lawler et al, 2014). This result points out the importance of including ISG emissions in global models. Regarding the *Base* run results, in general the *NoPhot* run reproduces the observations although in some regions the *Phot* scheme is closer to the measurements (Fig. 5). Note that the modelled IO vmr in the *Phot* scheme- likely to be a more realistic scheme for I_2O_x (Saiz-Lopez et al., 2014)- can even double the IO vmr given by the *NoPhot* scheme, stressing the need of further efforts from the community to investigate the fate of these higher iodine oxides. However, since the photolysis rates of I_2O_x are currently subject to uncertainty (Saiz-Lopez et al., 2014), hereafter only the *NoPhot* scheme is considered bearing, thus, the results presented as lower limits.

3.3 Sources of IO in the global marine boundary layer

After analysing the consistency of modelled vs. measured IO, in this section we investigate the sensitivity of the IO levels towards the different modelled iodine precursors. Considering the OSG emission inventory (Ordóñez et al., 2012) and the ISG (Prados-Roman et al., 2014), the modelled OSG/ISG ratio allows quantifying the individual sources and total oceanic emissions of iodine to the atmosphere. Results indicate that, globally averaged, the total oceanic iodine emissions yield 2.3 Tg y^{-1}. From these, only 17% (0.4 Tg y^{-1}) originate from organic sources, which are related to bacteria, microalgae, phytoplankton, etc. (Carpenter et al., 2012). On a global average, nearly half (43%) of the organic flux derives from CH_3I, 29% from CH_2ICl, 19% from CH_2I_2 and 9% from CH_2IBr, although their temporal and spatial distribution varies with, e.g., the solar radiation at sea surface and the properties of the ocean mixed layer (Bell et al., 2002; Carpenter et al., 2012; Ordóñez et al., 2012). The sea-air exchange of iodine is thus driven mainly by abiotic sources. Our results indicate that, globally averaged, 1.9 Tg (I) y^{-1} (i.e., 83% of the total oceanic iodine fluxes) are emitted to the MBL as a result of the reaction of tropospheric O_3 with I_{aq}^- in the ocean surface; and that the partitioning of these ISG emissions is directed by HOI (95% HOI, 5% I_2; Prados-Roman et al., 2014).

Figure 6a provides the annually averaged burden of IO in the global MBL, with values ranging from less than 0.05 pmol mol^{-1} in the sub-polar waters; to ~0.9 pmol mol^{-1} above waters offshore the Baja California peninsula. Figure 6b shows the geographical pattern of the contribution of ISG to the IO budget (i.e., IO_{ISG}). The model results indicate that, globally averaged, about 75% of the IO in the MBL derives from inorganic precursors. As mentioned

in the previous section, as an averaged value, this result is indeed consistent with previous estimates at given transects along the Pacific Ocean or offshore waters of Cape Verde and Galapagos Islands (Mahajan et al., 2010; Jones et al., 2010; Mahajan et al., 2012; Gómez Martín et al., 2013a; Großmann et al., 2013; Lawler et al, 2014). However, our model results show the uneven geographical distribution of IO_{ISG}, e.g., marine tropical regions in the southern hemisphere where IO_{ISG} is of 40%; or regions of ozone-related pollution outflow such the Bay of Bengal or the Gulf of Mexico (Myhre et al., 2013, see also SI) where, as a consequence of the O_3-I_{aq}^- interaction, IO_{ISG} can be more than 90%. Figure 7 shows the contribution of each of the four modelled iodocarbons to IO in the MBL, indicating that in the biological active regions of the tropics IO derives mainly from the dihalomethanes (CH_2ICl > CH_2I_2 > CH_2IBr) and to a lesser extend to CH_3I. Out of those regions CH_3I dominates the organic contribution to IO in the MBL, increasing with latitude as a result of its longer lifetime (Bell et al., 2002). Note however that the model simulations presented here do not include iodine emissions, organic or inorganic, from ice surfaces. Also, the strong dependence of the ISG flux with SST considerably reduces the inorganic iodine emissions over the cold waters in the high latitudes. Furthermore, as detailed in the study of MacDonald et al. (2014), the uncertainty on the parameterisation of ISG increases with decreasing SST. Thus, in the polar marine regions our simulated inorganic contribution to the IO budget should be regarded with caution. Despite these uncertainties, overall the main source of IO in the MBL at a global scale is HOI. However, as shown if Fig. 6b and Fig. 7, this is subject to strong spatial patterns in emission with regions in the southern hemisphere where the OSG can account for up to 50% of the modelled IO levels.

4 Summary

Here we present a comprehensive set of observations of iodine oxide mixing ratios in the marine boundary layer obtained after the Malaspina 2010 circumnavigation covering three non-polar oceans and both hemispheres. Complementing this dataset with measurements gained after campaigns in the tropical Atlantic Ocean and in the Eastern and Western Pacific Ocean, we provide field evidence for the ubiquitous presence of IO, and thus reactive iodine chemistry, in the global marine environment. By comparing these measurements with model results, we confirm the need of including the inorganic oceanic emissions of iodine into global models, and also stress the need for further laboratory and theoretical studies about the

atmospheric fate of I_2O_x. In particular, the model results indicate that 83% of the total oceanic natural emissions of iodine are inorganic (mainly HOI) following the reaction of iodide with ozone at the sea surface; and these inorganic emissions are indeed necessary to reproduce the observations of IO in all marine environments. Finally, our results show that the contribution of the organic/inorganic source gases to IO levels in the global MBL is geographically highly variable, existing regions of ozone-rich outflow where the inorganic contribution to IO can be more than 90%. This combined observational and modelling exercise strengthens the need of including both the organic and the inorganic oceanic emissions of iodine into global models for a more accurate assessment of the oxidizing capacity of the marine troposphere.

Acknowledgements

The authors would like to thank everyone involved in the Malaspina 2010 expedition, funded by the Spanish Ministry of Economy and Competitiveness. In particular the Marine Technology Unit (UTM-CSIC) for facilitating the ancillary data as well as the Hesperides R/V crew. We also thank Alan Thomas, John Robinson and Dave Humphries (NIWA) for building the MAX-DOAS tracker and the atmospheric group of the Institute of Environmental Physics (Heidelberg) for facilitating the gimbal table. We also thank Markus Rex for his comments on the ozone measurements during the TransBrom campaign, and Klaus Pfeilsticker and John Plane for helpful discussions. The Indian Institute of Tropical Meteorology is supported by the Ministry of Earth Sciences, Government of India. R.P.F would like to thank ANPCyT (PICT-PRH 2009-0063) for financial support. The data supporting this article can be requested from the corresponding author A.S-L (a.saiz@csic.es).

References

Barrie, L. A., Bottenheim, J. W., Schnell, R. C., Crutzen, P. J., and Rasmussen, R. A.: Ozone depletion and photochemical reactions at polar sunrise in the lower Arctic atmosphere, Nature, 334, 138-141, 1988.

Bell, N., Hsu, L., Jacob, D. J., Schultz, M. G., Blake, D. R., Butler, J. H., King, D. B., Lobert, J. M., and Maier-Reimer, E.: Methyl iodide: Atmospheric budget and use as a tracer of marine

convection in global models, Journal of Geophysical Research: Atmospheres, 107, 4340, 10.1029/2001JD001151, 2002.

Carpenter, L. J., Archer, S. D., and Beale, R.: Ocean-atmosphere trace gas exchange, Chem. Soc. Rev., 41, 6473-6506, 10.1039/C2CS35121H, 2012.

Carpenter, L. J., MacDonald, S. M., Shaw, M. D., Kumar, R., Saunders, R. W., Parthipan, R., Wilson, J., and Plane, J. M. C.: Atmospheric iodine levels influenced by sea surface emissions of inorganic iodine, Nature Geosci., 6, 108-111, 2013.

Chameides, W. L., and Davis, D. D.: Iodine: Its possible role in tropospheric photochemistry, J. Geophys. Res., 85, 7383-7398, 1980.

Draxler, R.R. and Rolph, G.D.: HYSPLIT (HYbrid Single-Particle Lagrangian Integrated Trajectory) Model access via NOAA ARL READY Website (http://ready.arl.noaa.gov/HYSPLIT.php). NOAA Air Resources Laboratory, Silver Spring, MD, 2014.

Garland, J. A., Elzerman, A. W., and Penkett, S. A.: The Mechanism for Dry Deposition of Ozone to Seawater Surfaces, J. Geophys. Res., 85, 7488-7492, 1980.

Gómez Martín, J. C., Mahajan, A. S., Hay, T. D., Prados-Román, C., Ordóñez, C., MacDonald, S. M., Plane, J. M. C., Sorribas, M., Gil, M., Paredes Mora, J. F., Agama Reyes, M. V., Oram, D. E., Leedham, E., and Saiz-Lopez, A.: Iodine chemistry in the eastern Pacific marine boundary layer, Journal of Geophysical Research: Atmospheres, 118, 887-904, 10.1002/jgrd.50132, 2013a.

Gómez Martín, J. C., Gálvez, O., Baeza-Romero, M. T., Ingham, T., Plane, J. M. C., and Blitz, M. A.: On the mechanism of iodine oxide particle formation, Phys. Chem. Chem. Phys., 15, 15612-15622, 10.1039/C3CP51217G, 2013b.

Großmann, K., Frieß, U., Peters, E., Wittrock, F., Lampel, J., Yilmaz, S., Tschritter, J., Sommariva, R., von Glasow, R., Quack, B., Krüger, K., Pfeilsticker, K., and Platt, U.: Iodine monoxide in the Western Pacific marine boundary layer, Atmos. Chem. Phys., 13, 3363-3378, 10.5194/acp-13-3363-2013, 2013.

Hönninger, G., Friedeburg, C. v., and Platt, U.: Multi axis differential optical absorption spectroscopy (MAX-DOAS), Atmos. Chem. Phys., 4, 231-254, 2004.

Jones, A. E., Anderson, P. S., Wolff, E. W., Roscoe, H. K., Marshall, G. J., Richter, A., Brough, N., and Colwell, S. R.: Vertical structure of Antarctic tropospheric ozone depletion events: characteristics and broader implications, Atmos. Chem. Phys., 10, 7775-7794, 10.5194/acp-10-7775-2010, 2010.

Lamarque, J. F., Emmons, L. K., Hess, P. G., Kinnison, D. E., Tilmes, S., Vitt, F., Heald, C. L., Holland, E. A., Lauritzen, P. H., Neu, J., Orlando, J. J., Rasch, P. J., and Tyndall, G. K.: CAM-chem: description and evaluation of interactive atmospheric chemistry in the Community Earth System Model, Geosci. Model Dev., 5, 369-411, 10.5194/gmd-5-369-2012, 2012.

Lawler, M. J., Mahajan, A. S., Saiz-Lopez, A., and Saltzman, E. S.: Observations of I_2 at a remote marine site, Atmos. Chem. Phys., 14, 2669-2678, 10.5194/acp-14-2669-2014, 2014.

MacDonald, S. M., Gómez Martín, J. C., Chance, R., Warriner, S., Saiz-Lopez, A., Carpenter, L. J., and Plane, J. M. C.: A laboratory characterisation of inorganic iodine emissions from the sea surface: dependence on oceanic variables and parameterisation for global modelling, Atmos. Chem. Phys., 14, 5841-5852, 10.5194/acp-14-5841-2014, 2014.

Mahajan, A. S., Plane, J. M. C., Oetjen, H., Mendes, L., Saunders, R. W., Saiz-Lopez, A., Jones, C. E., Carpenter, L. J., and McFiggans, G. B.: Measurement and modelling of tropospheric reactive halogen species over the tropical Atlantic Ocean, Atmos. Chem. Phys., 10, 4611-4624, 10.5194/acp-10-4611-2010, 2010.

Mahajan, A. S., Gómez Martín, J. C., Hay, T. D., Royer, S. J., Yvon-Lewis, S., Liu, Y., Hu, L., Prados-Roman, C., Ordóñez, C., Plane, J. M. C., and Saiz-Lopez, A.: Latitudinal distribution of reactive iodine in the Eastern Pacific and its link to open ocean sources, Atmos. Chem. Phys., 12, 11609-11617, 10.5194/acp-12-11609-2012, 2012.

Mahajan, A. S., Prados-Roman, C., Hay, T. D., Lampel, J., Pöhler, D., Groβmann, K., Tschritter, J., Frieß, U., Platt, U., Johnston, P., Kreher, K., Wittrock, F., Burrows, J. P., Plane, J. M. C., and Saiz-Lopez, A.: Glyoxal observations in the global marine boundary layer, Journal of Geophysical Research: Atmospheres, 119, 2013JD021388, 10.1002/2013JD021388, 2014.

Molina, M. J., and Rowland, F. S.: Stratospheric sink for chlorofluoromethanes: Chlorine-atom catalysed destruction of ozone, Nature, 249, 810-812, 1974.

Myhre, G., D. Shindell, D., Bréon, F.-M., Collins, W., Fuglestvedt, J., Huang, J., Koch, D., Lamarque, J.-F., Lee, D., Mendoza, B., Nakajima, T., Robock, A., Stephens, G., Takemura, T. and Zhang, H.: Anthropogenic and Natural Radiative Forcing. In: Climate Change 2013: The Physical Science Basis. Contribution of Working Group I to the Fifth Assessment Report of the Intergovernmental Panel on Climate Change [Stocker, T.F., D. Qin, G.-K. Plattner, M. Tignor, S.K. Allen, J. Boschung, A. Nauels, Y. Xia, V. Bex and P.M. Midgley (eds.)]. Cambridge University Press, Cambridge, United Kingdom and New York, NY, USA, Chap. 8, 2013.

Ordóñez, C., Lamarque, J. F., Tilmes, S., Kinnison, D. E., Atlas, E. L., Blake, D. R., Sousa Santos, G., Brasseur, G., and Saiz-Lopez, A.: Bromine and iodine chemistry in a global chemistry-climate model: description and evaluation of very short-lived oceanic sources, Atmos. Chem. Phys., 12, 1423-1447, 10.5194/acp-12-1423-2012, 2012.

Platt, U., and Stutz, J.: Differential Absorption Spectroscopy, in: Differential Optical Absorption Spectroscopy, Physics of Earth and Space Environments, Springer, Berlin Heidelberg, 135-174, 2008.

Prados-Roman, C., Cuevas, C., Fernandez, R. P., Kinnison, D. E., Lamarque, J-F., and Saiz-Lopez, A.: A negative feedback between anthropogenic ozone pollution and enhanced ocean emissions of iodine, accepted for ACPD, 2014.

Rayner, N. A., Parker, D. E., Horton, E. B., Folland, C. K., Alexander, L. V., Rowell, D. P., Kent, E. C., and Kaplan, A.: Global analyses of sea surface temperature, sea ice, and night marine air temperature since the late nineteenth century, Journal of Geophysical Research: Atmospheres, 108, 4407, 10.1029/2002JD002670, 2003.

Read, K. A., Mahajan, A. S., Carpenter, L. J., Evans, M. J., Faria, B. V. E., Heard, D. E., Hopkins, J. R., Lee, J. D., Moller, S. J., Lewis, A. C., Mendes, L., McQuaid, J. B., Oetjen, H., Saiz-Lopez, A., Pilling, M. J., and Plane, J. M. C.: Extensive halogen-mediated ozone destruction over the tropical Atlantic Ocean, Nature, 453, 1232-1235, 2008.

Saiz-Lopez, A., Plane, J. M. C., Mahajan, A. S., Anderson, P. S., Bauguitte, S. J.-B., Jones, A. E., Roscoe, H. K., Salmon, R. A., Bloss, W. J., Lee, J. D., and Heard, D. E.: On the vertical distribution of boundary layer halogens over coastal Antarctica: implications for O_3, HO_x, NO_x and the Hg lifetime, Atmos. Chem. Phys., 8, 887-900, 2008.

Saiz-Lopez, A., and von Glasow, R.: Reactive halogen chemistry in the troposphere, Chem. Soc. Rev., 41, 6448-6472, 10.1039/C2CS35208G, 2012.

Saiz-Lopez, A., Plane, J. M. C., Baker, A. R., Carpenter, L. J., Von Glasow, R., Gómez Martín, J. C., McFiggans, G., and Saunders, R. W.: Atmospheric Chemistry of Iodine, Chem. Rev. (Washington, DC, U. S.), 112, 1773-1804, 10.1021/cr200029u, 2012.

Saiz-Lopez, A., Fernandez, R. P., Ordóñez, C., Kinnison, D. E., Gómez Martín, J. C., Lamarque, J. F., and Tilmes, S.: Iodine chemistry in the troposphere and its effect on ozone, Atmos. Chem. Phys. Discuss., 14, 19985-20044, 10.5194/acpd-14-19985-2014, 2014.

Wagner, T., Dix, B., Friedeburg, C. v., Frieß, U., Sanghavi, S., Sinreich, R., and Platt, U.: MAX-DOAS O_4 measurements: A new technique to derive information on atmospheric aerosols—Principles and information content, Journal of Geophysical Research: Atmospheres, 109, D22205, 10.1029/2004JD004904, 2004.

Table 1. Description of the different legs of the Malaspina 2010 expedition. Due to technical problems, the O_3 and IO measurements presented in this work correspond to the period from 21/02/2011 to 12/07/2011.

Legs	**Docking places**	**Docking dates (dd/mm/yyyy)**
1	Cadiz (Spain) - Rio de Janeiro (Brazil)	14/12/2010-13/01/2011
2	Rio de Janeiro (Brazil) – Cape Town (South Africa)	17/01/2011-06/02/2011
3	Cape Town (South Africa) – Perth (Australia) – Sydney (Australia)	11/02/2011-13/03/2011-30/03/2011
4	Sydney (Australia) – Auckland (New Zealand) – Honolulu (Hawaii)	04/04/2011-13/04/2011-08/05/2011
5	Honolulu (Hawaii) – Panama (Panama) - Cartagena de Indias (Colombia)	13/05/2011-10/06/2011-13/06/2011
6	Cartagena de Indias (Colombia) – Cartagena (Spain)	19/06/2011-14/07/2011

Table 2. Summary of the O_3 and ancillary parameters measured during Malaspina 2010. The data correspond to daytime average values concurrent with the IO measurements gathered during the expedition (Fig. 1).

Parameter	**Mean**	**Std**	**Minimum**	**Maximum**
O_3 (nmol mol^{-1})	16.0	9.4	3.4	42.4
ws (m s^{-1})	7.0	2.0	3.3	11.6
SST (K)	298.9	2.9	291.6	303.0

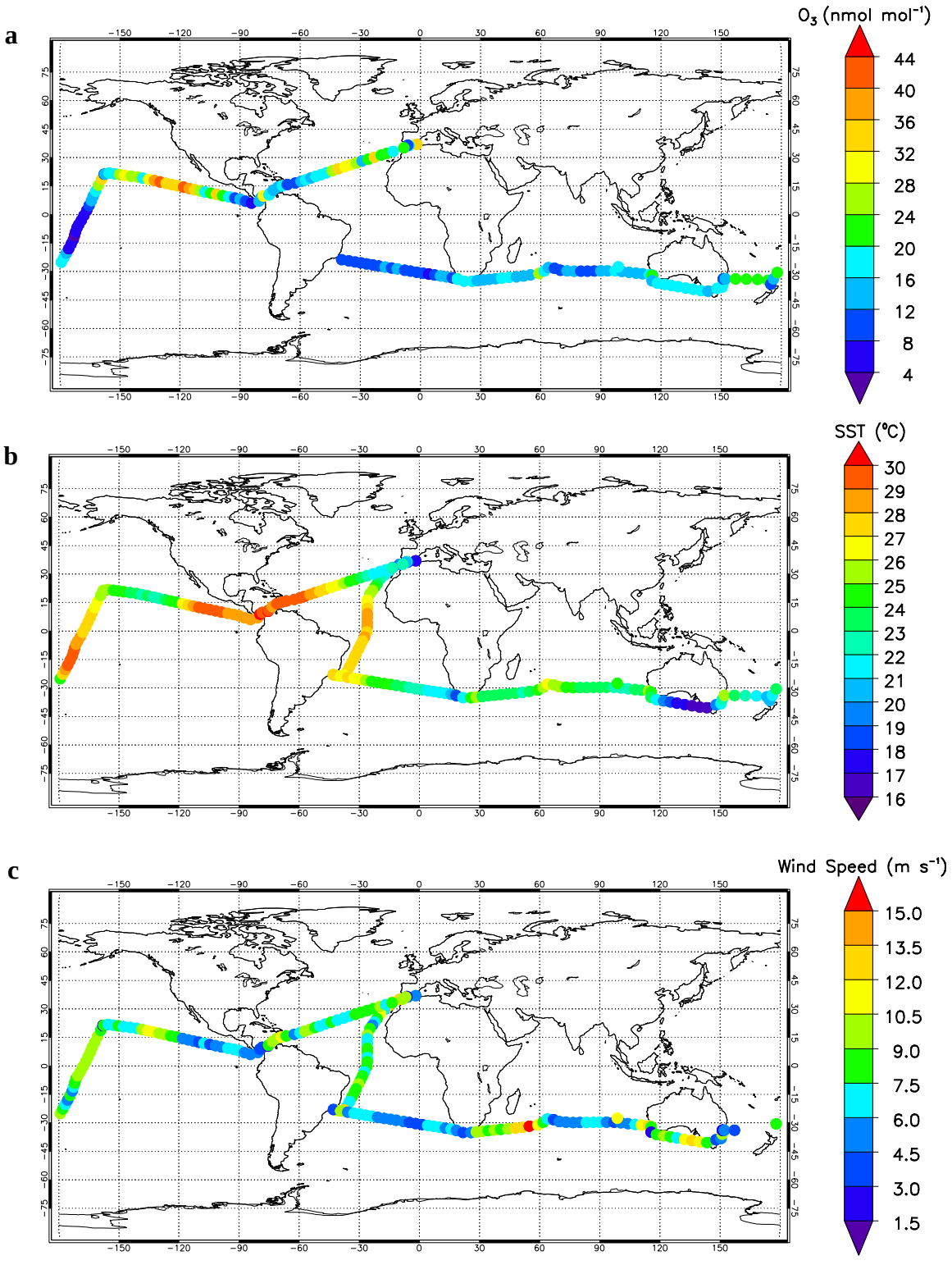

Figure 1. Observations of surface ozone and ancillary parameters during Malaspina 2010 (daily average). a. O_3 mixing ratios. b. Sea surface temperature. c. Wind speed. See also Table 2.

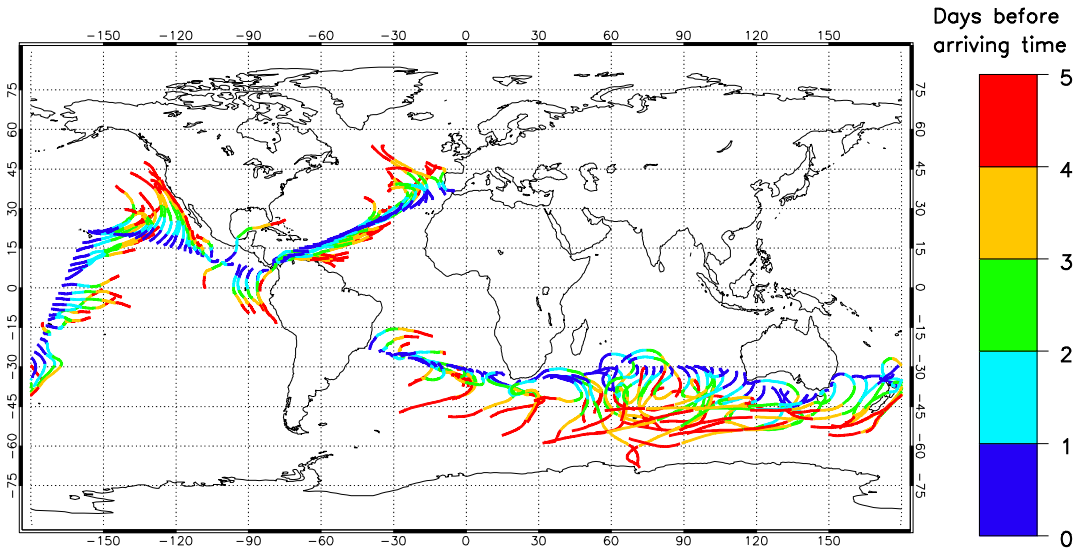

Figure 2. Backward trajectories of the air masses arriving at noon on every day of the Malaspina's cruise. They were calculated using HYbrid Single-Particle Lagrangian Integrated Trajectory (HYSPLIT, Draxler and Rolph, 2014).

a

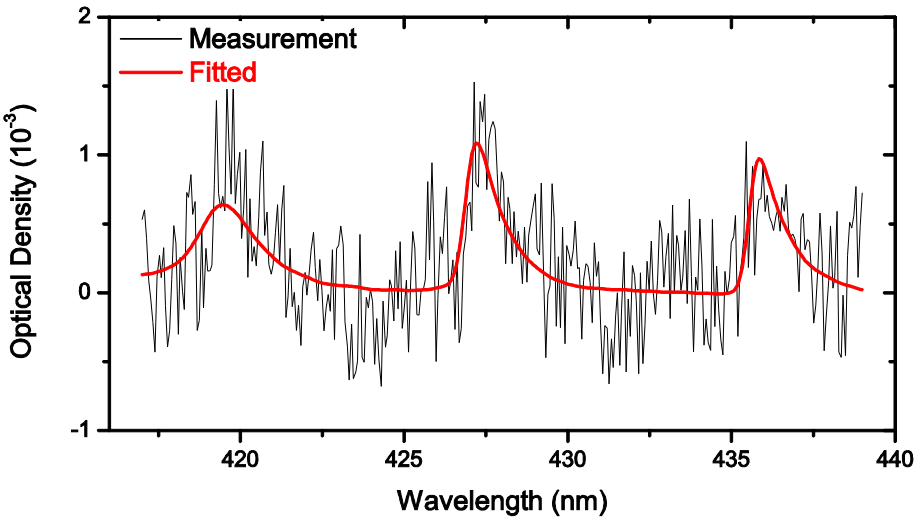

1

b

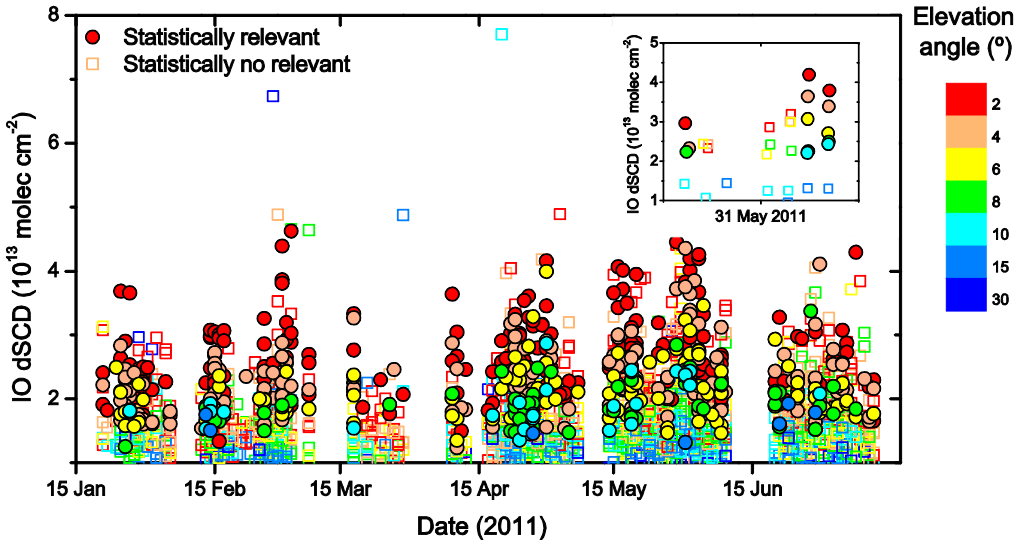

2

3 Figure 3. Retrieval of IO during the Malaspina 2010 circumnavigation. a. Example of a
4 typical IO spectral fit during the expedition. The particular spectrum was taken on the 31st of
5 May 2011 (3pm LT, 53º SZA) in the Eastern Pacific for a 2º elevation angle. The black line
6 represents the measured IO optical density and the red line the retrieved one after the DOAS
7 retrieval. This fit resulted in an IO dSCD of (3.8 ± 0.3) x10^{13} molecules cm^{-2} (i.e., IO vmr of
8 0.8 ± 0.1 pmol mol^{-1}), with a residual optical density of 3.9x10^{-4} (root mean square). b.
9 Timeline of the IO dSCD observed during the expedition. Statistically relevant data (i.e., data
10 above the quality filters, SI) are shown with filled circles, and the non relevant data with

empty squares. The inset shows the daily evolution of IO dSCD for the 31st of May 2011. The colour code indicates the elevation angle of the measurements.

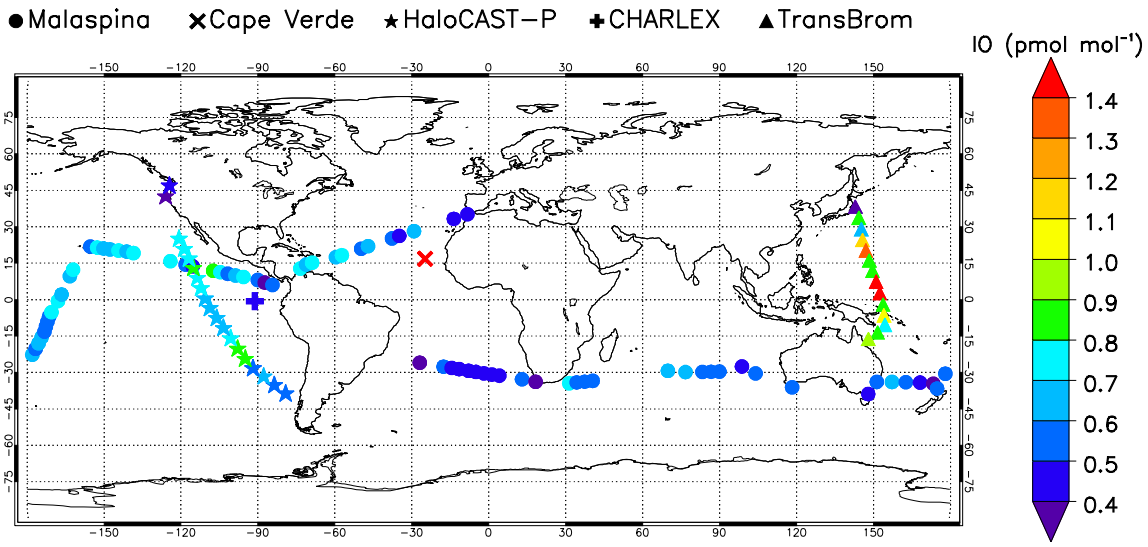

Figure 4**.** Iodine oxide observations in the global marine boundary layer. IO mixing ratios (in pmol mol^{-1}) are shown for five different field campaigns (Malaspina (this work), CHARLEX (Gómez Martín et al., 2013a), TransBrom (Großmann et al., 2013), HaloCAST-P (Mahajan et al., 2012), and Cape Verde (Read et al., 2008; Mahajan et al., 2010). For the three ship campaigns (Malaspina, HaloCAST-P and TransBrom) daytime averaged values are shown. For the long-term measurements on the Galapagos and the Cape Verde Islands (referred to as CHARLEX and Cape Verde, respectively), the mean daytime IO values observed throughout the campaigns are given.

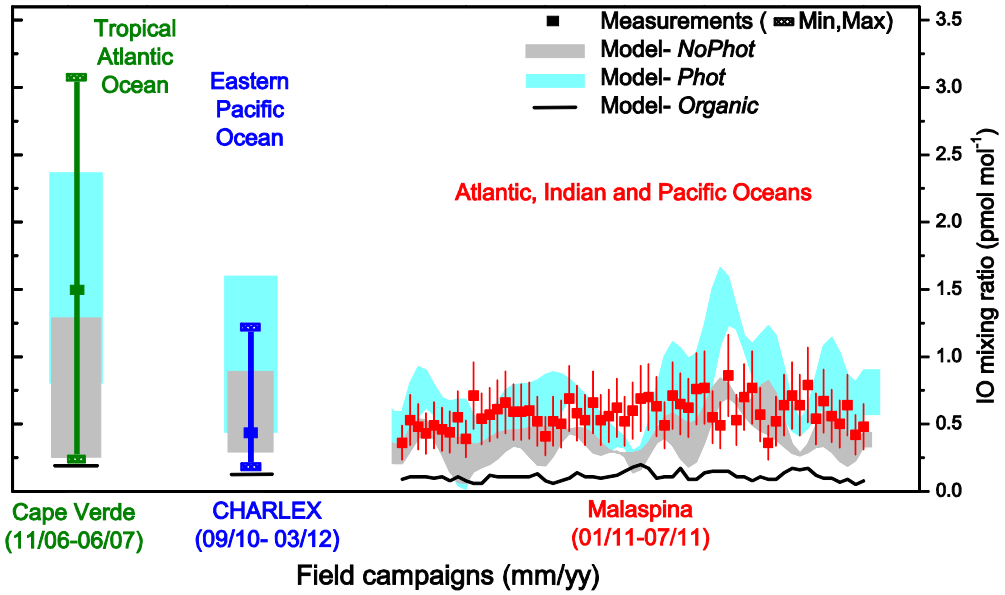

Figure 5. Measured and modelled IO mixing ratios in different field campaigns and oceans. For the two long-term campaigns on islands (Cape Verde- in green- and CHARLEX- in blue) the mean daytime IO mixing ratio observed during the whole campaign period is given (filled squares), together with the minimum and maximum observed values (dashed rectangles) (Read et al., 2008; Mahajan et al., 2010; Jones et al., 2010). In the case of the Malaspina circumnavigation (in red), daytime averaged IO mixing ratios are provided (filled squares) along with their error (see also the SI). The shaded areas represent the standard deviation of the modelled fields for the *NoPhot* (gray) and *Phot* (cyan) *Base* scheme. For comparison purposes the IO vmr modelled considering only the organic iodine precursors (*Organic* run) are also included (solid black line).

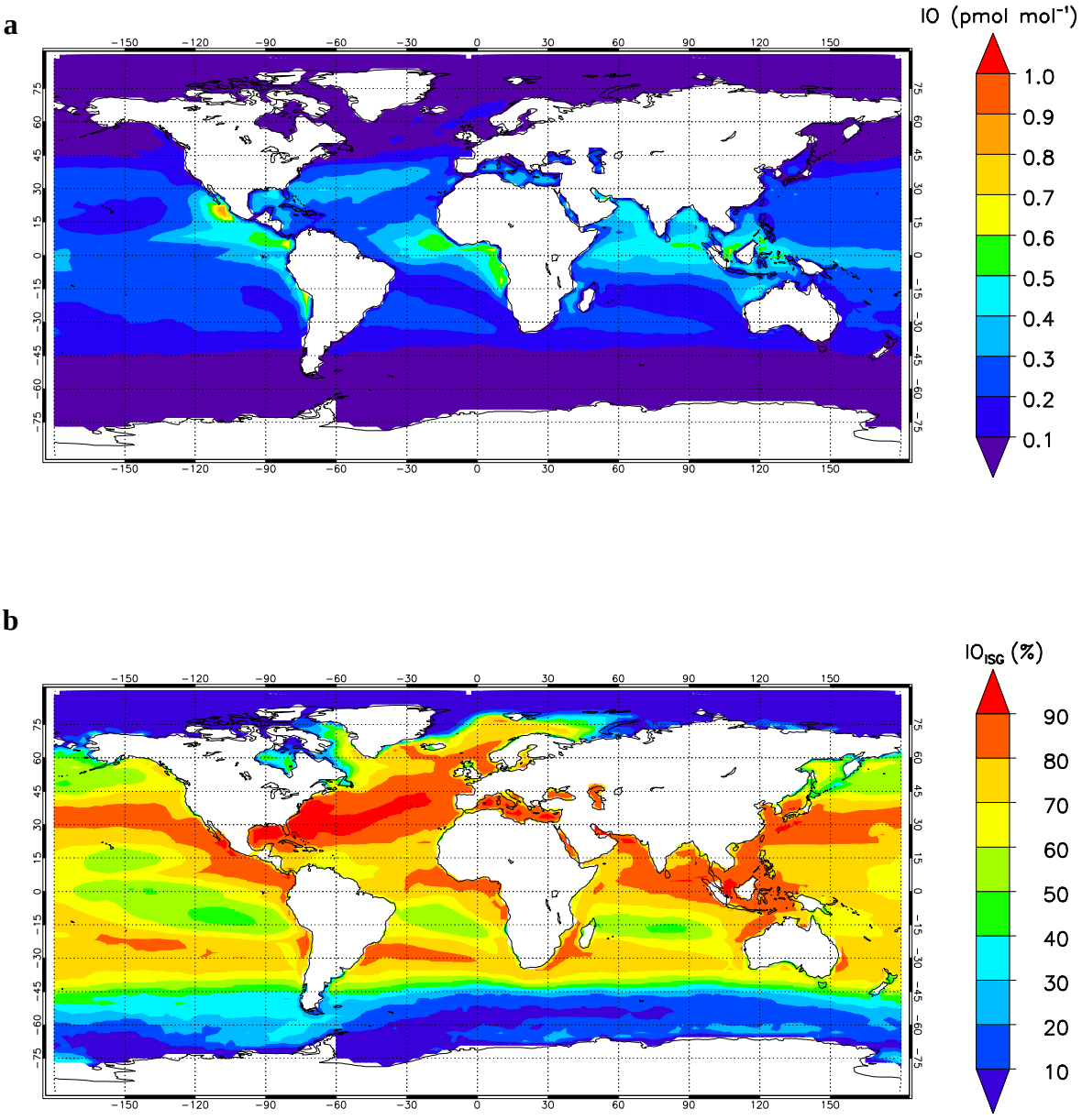

Figure 6. Simulated IO in the global marine environment (annually averaged). a. Geographical distribution of the total IO budget in the MBL (i.e., $IO_{ISG+OSG}$), in units of vmr (pmol mol^{-1}). b. Percentage contribution of the ISG emissions to the budget of IO in the global MBL.

a

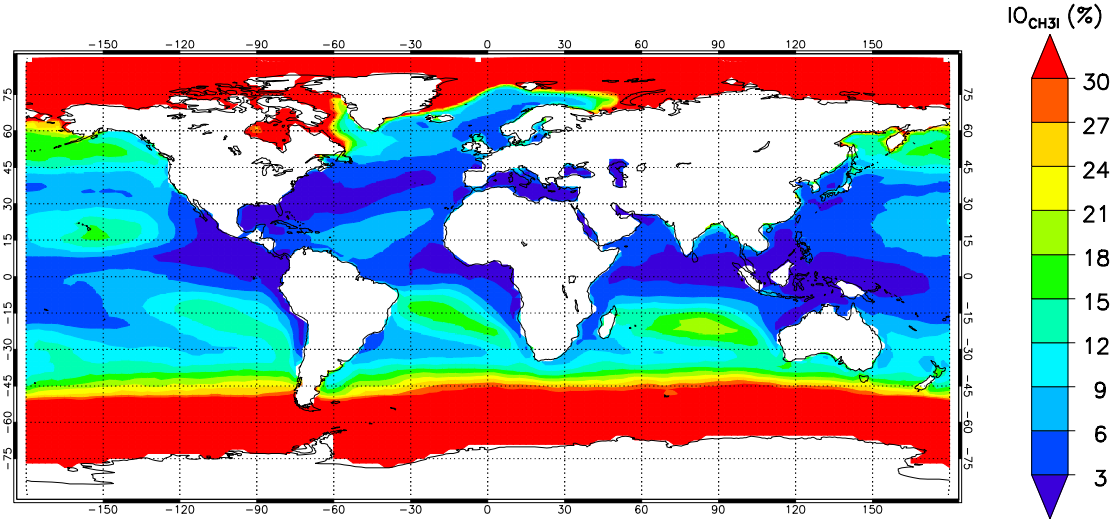

1

b

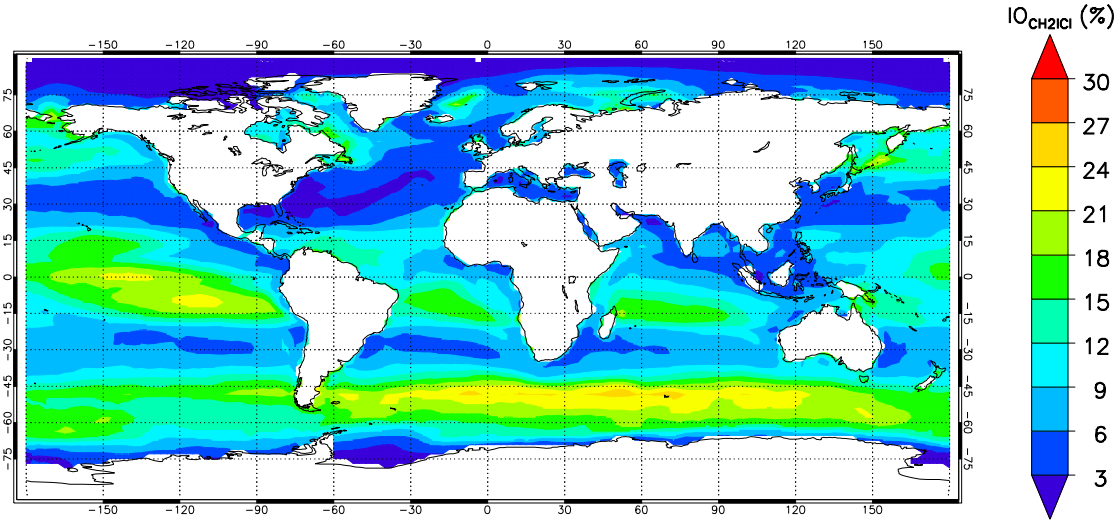

2

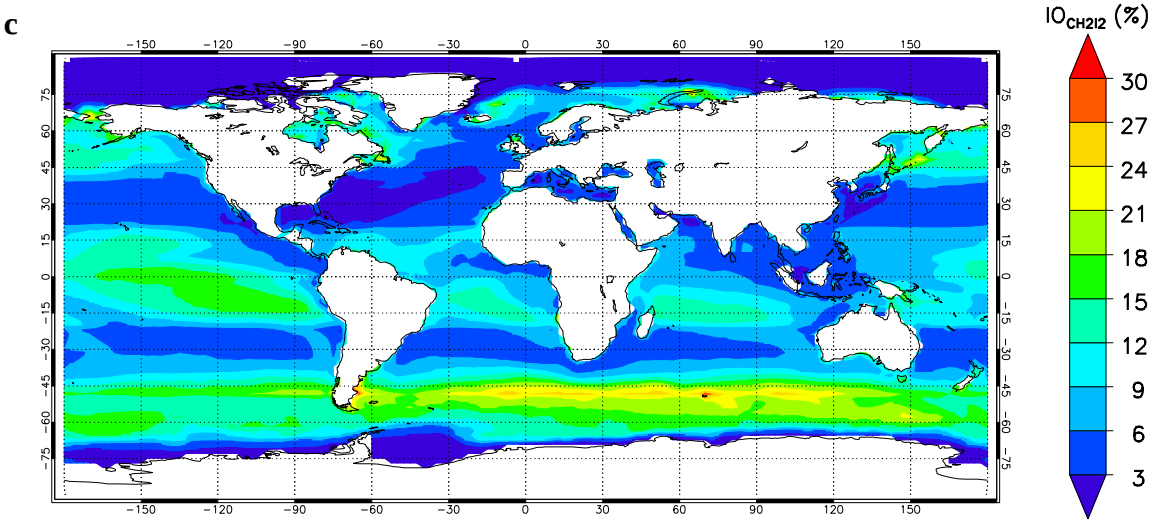

1

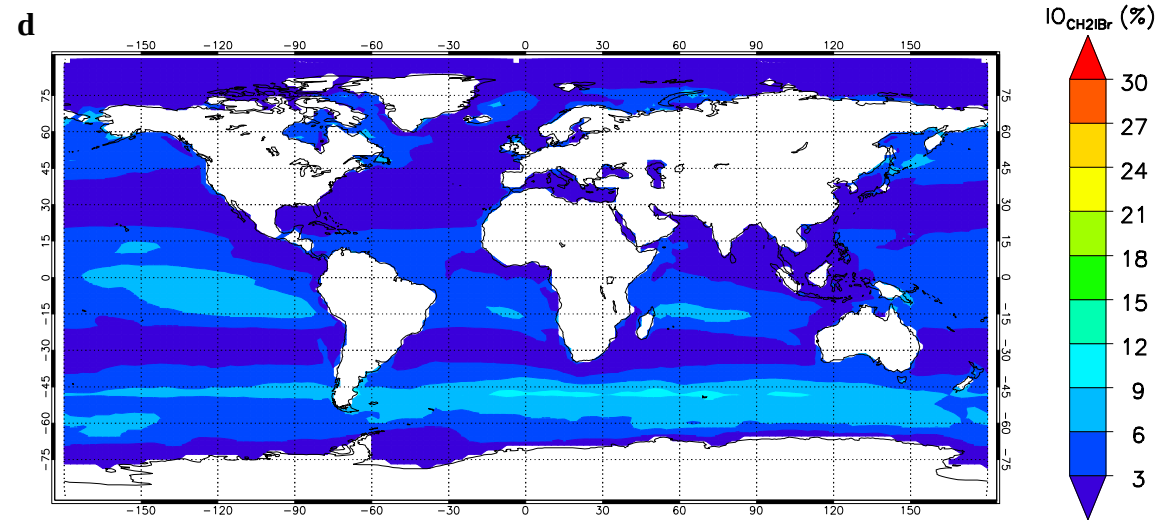

2

3 Figure 7. Simulated percentage contribution of the different short-lived iodocarbons (a. CH_3I.
4 b. CH_2ICl. c. CH_2I_2. d. CH_2IBr) to the IO budget in the marine environment. Note that, for
5 comparison purposes, the colour code is the same in the four panels. Also note that these
6 model simulations do not include iodine emissions from ice surfaces. For the absolute values
7 of the OSG emissions, please refer to the study of Ordóñez et al., 2012.

8

Supplementary Information

Iodine oxide in the global marine boundary layer

1 Methods

1.1 Measurements of IO during Malaspina 2010

1.1.1 Spectral retrieval of IO

The analysis of IO on the 417-439 nm spectral region was performed as described in the study of Mahajan et al. (2012), with the updated H_2O water cross-section (Rothman et al, 2013). Glyoxal (CHOCHO) was not included in the spectral fit of IO since CHOCHO was under the instrumental detection limit (Mahajan et al., 2014). Aiming at increasing the signal-to-noise ratio, spectra were accumulated during 1 h, resulting in a residual root-mean-square (RMS) of 2–6 $x10^{-4}$ and a mean 2σ detection limit of 1.2-3.5 $x10^{13}$ molecules cm^{-2} for IO. An example of a typical spectral fit of IO is shown in Fig. 3a.

Similar to previous studies (Sinreich et al., 2010; Mahajan et al., 2012; Gómez Martín et al., 2013a; Großmann et al., 2013), the following filters were included in the DOAS data analysis for quality assurance:

- The data collected at SZA>60º were excluded in the analysis (minimizing possible contribution of stratospheric trace gases).
- Saturated spectra that occurred around noon at some locations were also excluded before the DOAS analysis.
- The upper limit allowed for the RMS of the DOAS fit was of 10^{-3}.
- A wind direction filter was applied, preventing data in which the ship's exhaust plume crossed the MAX-DOAS field-of-view.
- A cloud filter was also introduced based on in-situ measured solar radiation and radiances measured at the edges of the chip of the CCD camera of the MAX-DOAS (400 and 480 nm in this case). With this cloud filter a threshold for the cloud-free scenario was set, assuring therefore consistency in the scattering conditions between all the data measured under clear sky. An example of this filter is shown in Fig. S1.

For additional details on this cloud filter please refer to the previous works of, e.g., Sinreich et al. (2010); Mahajan et al. (2012) or Gómez Martín et al. (2013a).

- In order to assure measurements representative of open marine conditions, data collected while the vessel was in a harbour or close to it were excluded from the data set.

Data above/below these quality filters were considered statistically relevant/irrelevant as presented in Fig. 3b. Only statistically relevant data were used for the retrieval of IO vmr.

1.1.2 Retrieval of IO mixing ratios

Following the approach of previous studies (e.g., Sinreich et al., 2010; Mahajan et al., 2012; Gómez Martín et al., 2013a), the IO mixing ratios along the ship track were inferred from the measured IO dSCD applying the *O_4 method* (Wagner et al., 2004; Frieß et al., 2006) after validating that method with the IO mixing ratios inferred by the *inversion method*, i.e., by means of a RTM (NIMO, Hay et al. (2012)) combined with the optimal estimation approach (Rodgers, 2000). Since the *O_4 method* and the *inversion method* have been both widely used for retrieving mixing ratios in the MBL, no details on the methods are provided herein. For the rationale and further details behind either of these methods, please refer to the above mentioned references.

Briefly, in the *O_4 method* the atmospheric scattering conditions are characterised and, consequently, the light path needed to infer mixing ratios from dSCD. In order to retrieve the IO mixing ratios by applying this method, the O_4 dSCD along the Malaspina's ship track were measured in the 338-370 nm spectral region. For this vmr retrieval exercise, only the dSCD for the 2º elevation angle (α) were used and a scaling factor was applied to transfer the scattering conditions inferred in the UV to the spectral range of IO (further details in Mahajan et al., 2012; Gómez Martín et al., 2013a). Sensitivity studies performed with the NIMO RTM (Hay et al., 2012) with data collected along the cruise indicated a last scattering altitude between 250-1300 m for $\alpha = 2^o$, with 600 m as the mean last scattering altitude (LSA) of the photon reaching the detector at that elevation angle defining the upper layer of the sensed "column" (i.e., MBL). Hence the IO mixing ratios obtained through the *O_4 method* should be regarded as an averaged value within the first 600 m of the troposphere. Similarly, the degrees of freedom (0.6-0.8) and averaging kernels obtained after applying the *inversion method* indicated that the retrieved IO vmr vertical profile was smoothed in the first 600-800 m, therefore not gaining any additional information by applying the costly *inversion method*.

Nevertheless, for validation purposes, vertical profiles of IO vmr were inferred by the *inversion approach* for several days during the different legs of the circumnavigation. For this *inversion approach*, in order to characterise the scattering properties of the atmosphere, a vertical profile of the aerosol extinction coefficient (EC) was previously inferred through forward modelling O_4 dSCD (Wagner et al., 2004; Frieß et al., 2006). An example of the derived aerosol EC is shown in Fig. S2a, with a vertical profile decreasing rapidly with height. Note that the MAX-DOAS instrument during Malaspina 2010 was placed at ~10 m.a.s.l and no measurements were performed at negative elevation angles. Hence the EC inferred below that altitude should be regarded with caution. Nevertheless in all cases only an aerosol EC vertical profile type as Fig. S2 –with relatively high values up to 10 m altitude and virtually zero above 30 m- could reproduce measured O_4 dSCD for all elevation angles. This sort of EC profile was included in the model in order to invert the IO vmr vertical profiles. Based on previous works (e.g. Mahajan et al., 2012) the surface albedo used in the RTM was of 7% and the aerosols were assumed to be of marine origin (asymmetry parameter 0.75 and single scattering albedo 0.97). The vertical grid for the vmr inversion exercise was of 100 m. Examples of the inverted IO vmr through this *inversion approach* are shown in Fig. S2b.

Figure S3 provides the comparison of the IO vmr obtained from the *O_4 method* and from the *inversion approach* considering the modelled LSA = 600 m altitude. As shown in the figure, the IO vmr inferred with both methods showed a good agreement with more than 99% confidence, although values gained after the *O_4 method* overestimated the IO vmr by about 15%. That factor was hence applied to the *O_4 method*-derived IO vmr reported in this study.

Error analysis

Herein we discuss the error characterisation of the IO vmr inferred by both methods. In Fig. S3, the error bars of the IO vmr inferred through the *inversion method* derive from the optimal estimation equations (Rodgers, 2000), being the measurement error (18%) the dominant error source. The error related to the IO vmr derived from the *O_4 method* is rather complex to estimate given the different assumptions related to the method itself such as a similar shape of the vertical profile of IO and O_4, or the presence of a homogenous IO layer until the last scattering altitude (e.g., Wagner et al., 2004; Mahajan et al., 2012; Gómez Martín et al., 2013a). The IO vmr values reported in the main text were obtained through this *O_4 method* and the error bars provided (Fig. 5 and Fig. S3) derived from the IO and O_4 dSCD measurement errors and from forward RTM modelling sensitivity studies for different aerosol

loads and IO profile shapes. Overall, we estimated a 30% uncertainty for the retrieved IO vmr reported in this work, albeit probably underestimated.

1.2 Ancillary data during Malaspina 2010: measurements vs. model

Since the newly included formulation of ISG in the CAM-Chem model depends on O_3, wind speed and sea surface temperature (Carpenter et al., 2013; MacDonald et al., 2014), aiming at testing the model performance, we compared observations of those parameters observed during Malaspina 2010 with the modelled ones. Figure S4 shows the comparison of the modelled daily averages (9:00-17:00 LT) of the three parameters computed for each Malaspina's time and geolocation, with daytime values observed during the cruise in the period where IO was also observed. As shown in the figure, the model climatology reproduces well the experimental measurements, with relative deviations smaller than 15%. From the three parameters, SST showed the best representation with R^2=0.91 and 99.9% confidence. Note that wind speeds measured along the Malaspina's transect were above the threshold of 3 m s^{-1} set by MacDonald et al. (2014) for the validity of the ISG parameterisation. Further discussions on the intrinsic limitations and uncertainties of the parameterisation of ISG flux are addressed elsewhere (Carpenter et al., 2013; MacDonald et al., 2014; Prados-Roman et al., 2014).

1.3 Modelled O_3 in the global marine environment

For completeness of results shown in the main text, Fig. S5 provides the globally modelled O_3 mixing ratios. Modelled values and spatial distribution agree with observations (e.g., Myhre et al., 2013).

References unique to this SI

Frieß, U., Monks, P. S., Remedios, J. J., Rozanov, A., Sinreich, R., Wagner, T., and Platt, U.: MAX-DOAS O_4 measurements: A new technique to derive information on atmospheric aerosols: 2. Modeling studies, J. Geophys. Res.,: Atmospheres, 111, D14203, 10.1029/2005JD006618, 2006.

Hay, T. D., Bodeker, G. E., Kreher, K., Schofield, R., Liley, J. B., Scherer, M., and McDonald, A. J.: The NIMO Monte Carlo model for box-air-mass factor and radiance calculations, Journal of Quantitative Spectroscopy and Radiative Transfer, 113, 721-738, http://dx.doi.org/10.1016/j.jqsrt.2012.02.005, 2012.

Rodgers, C. D.: Inverse methods for atmospheric sounding: Theory and Practice, Series on Atmospheric, Oceanic and Planetary Physics–Vol. 2, Singapore, World Scientific, 2000.

Rothman, L. S. et al.: The HITRAN 2012 molecular spectroscopic database. JQSTR 130, 4-50, 2013.

Sinreich, R., Coburn, S., Dix, B., and Volkamer, R.: Ship-based detection of glyoxal over the remote tropical Pacific Ocean, Atmos. Chem. Phys., 10, 11359-11371, doi:10.5194/acp-10-11359-2010, 2010.

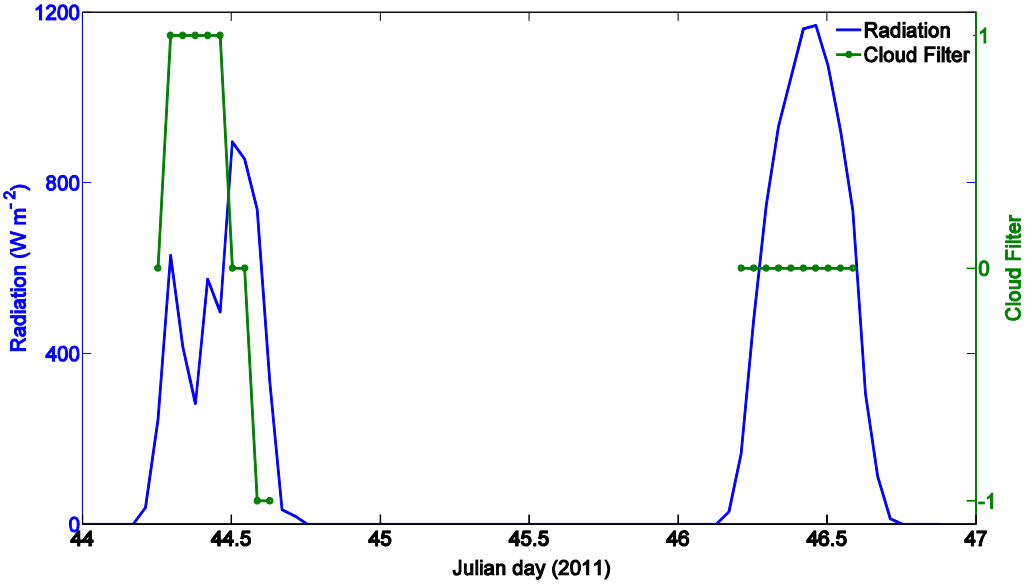

Figure S1. Example of the cloud filter applied in the Malaspina dataset. The left axis indicates the in-situ measured radiation (in blue). The right axis corresponds to the cloud filter (in green) and indicates cloud-free conditions for 0, cloudy conditions for 1 and missing data for -1 (neglected therefore).

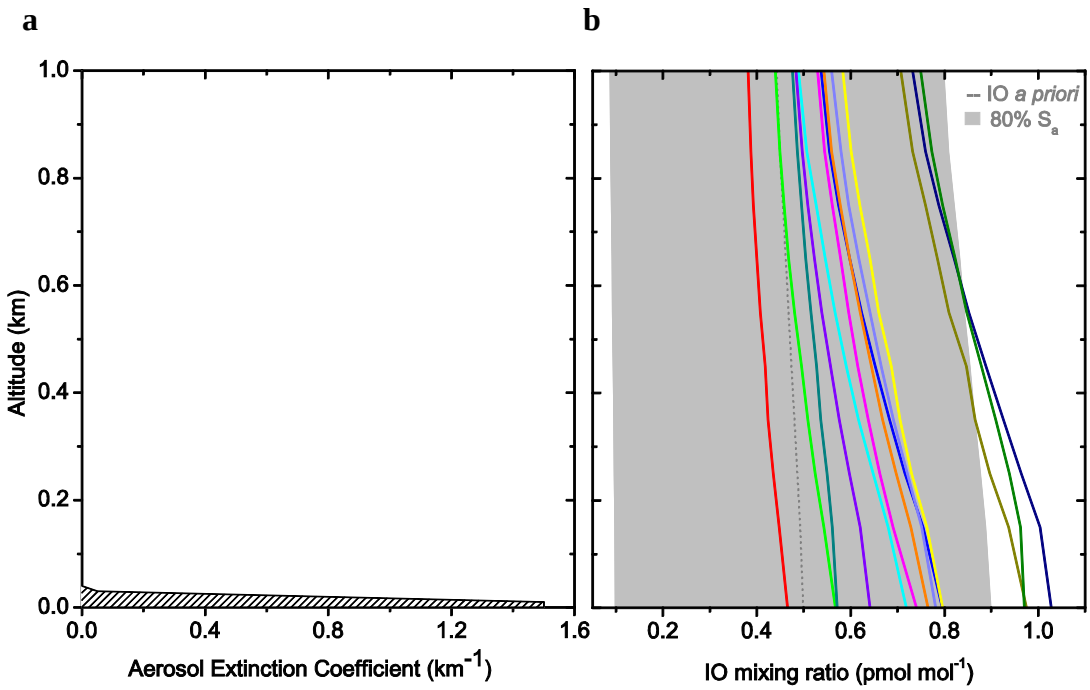

1

2 Figure S2. Inversion method for retrieving vertical profiles of IO mixing ratios. a. In
3 consistency with previous works (Mahajan et al., 2012; Gómez Martín et al., 2013a), this
4 panels shows the typical aerosol extinction coefficient considered in the RTM (inferred after
5 O_4 dSCD forward modelling) for the inversion of IO vmr vertical profiles. b. Profiles of IO
6 vmr inverted in the first kilometre of the MBL for several days during Malaspina 2010. The
7 dashed gray line is the a priori IO used, with its covariance indicated by the gray shadow. The
8 solid lines show the IO vmr profiles inverted (100 m vertical grid).

9

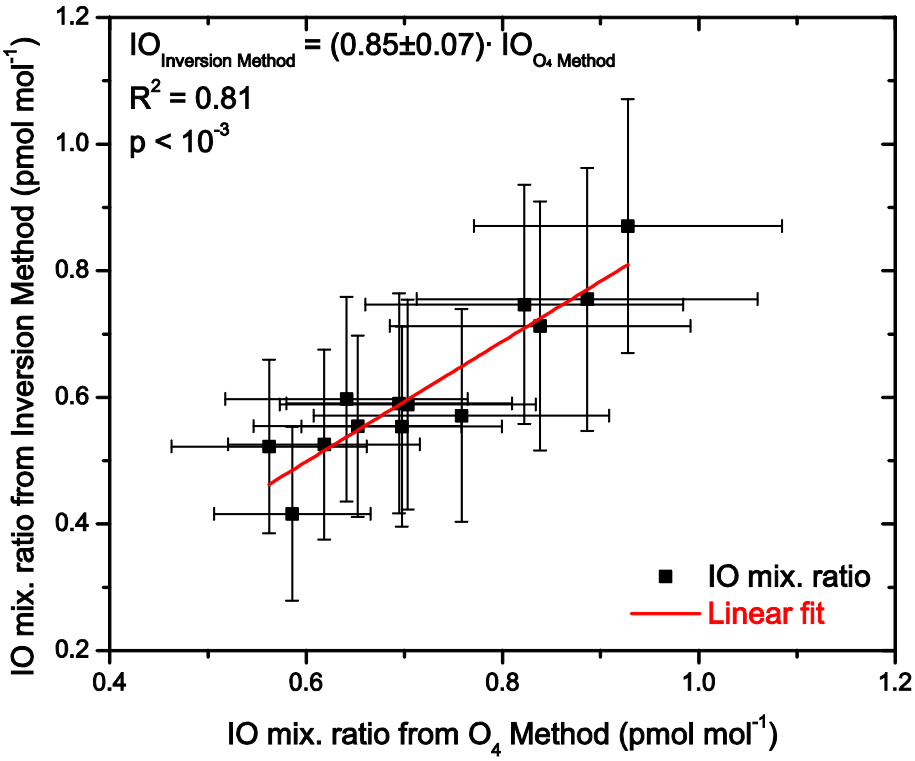

Figure S3. Comparison of the IO mixing ratios along the Malaspina's transect derived from the *O_4 method* and from the *inversion approach*. The linear fit (dashed gray line) of the inverted mixing ratios (black squares) indicates a high correlation between the two retrieval methods, with a confidence level higher than 99%.

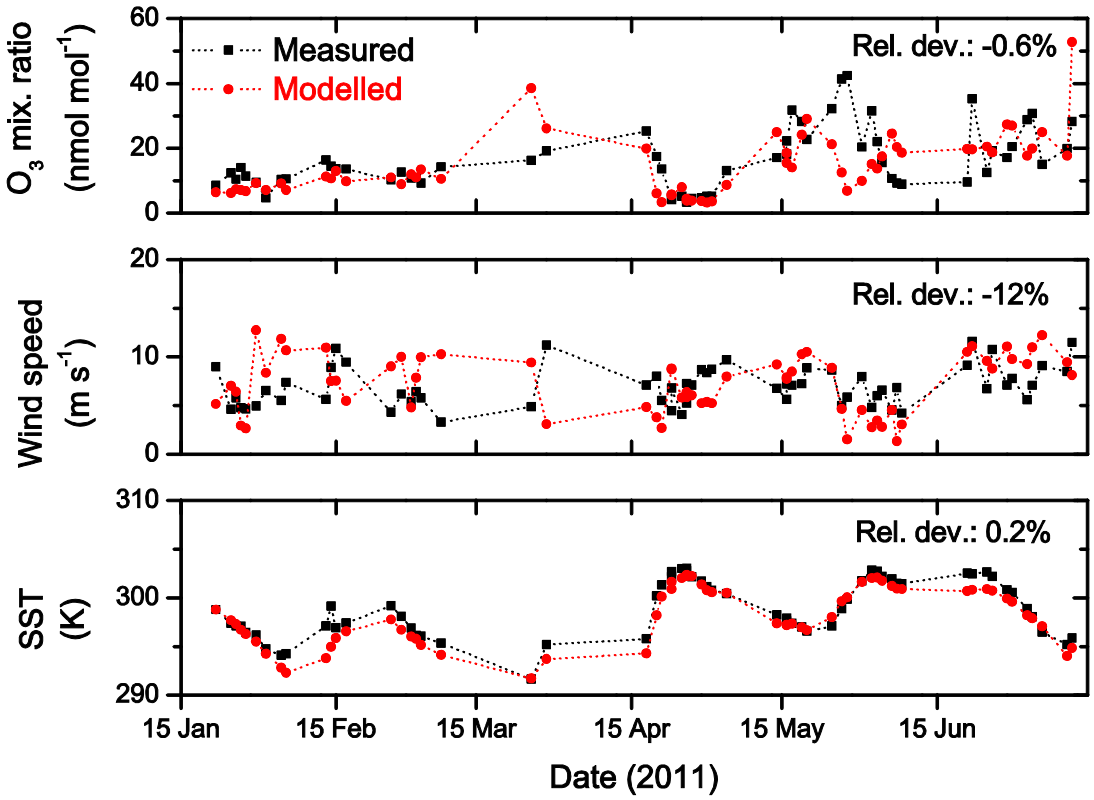

1

2 Figure S4. Measured and modelled daytime values of surface O_3 mixing ratios (upper panel),
3 wind speed (middle panel) and sea surface temperature (SST, lower panel) during the
4 Malaspina campaign. The relative deviation of each modelled values (i.e., difference of the
5 measured and modelled values relative to measured ones) is also provided as "Rel. dev.".

6

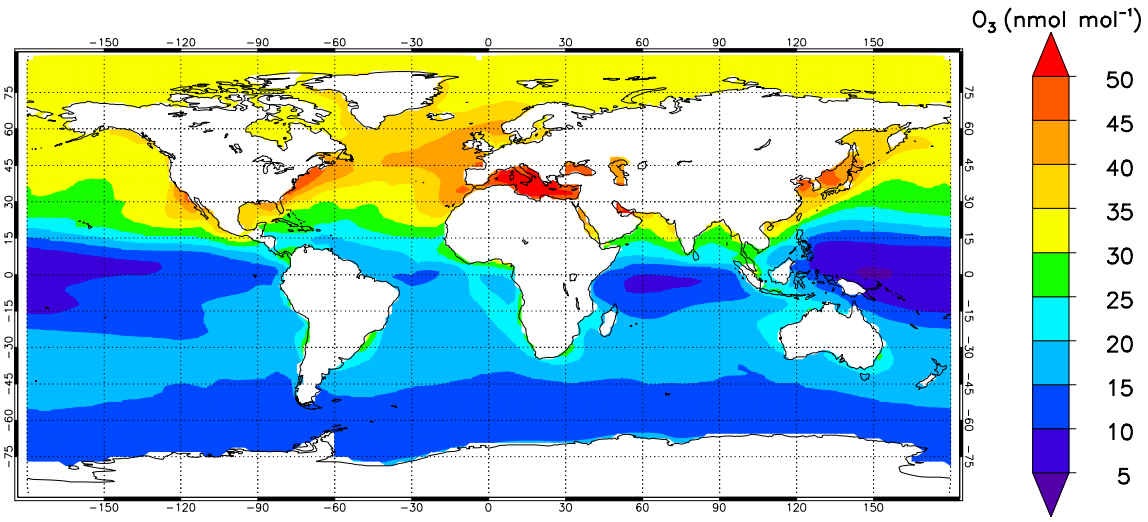

1

2 Figure S5. Modelled annual averaged surface ozone mixing ratios in the marine environment.